ADVANCED FUNCTIONAL MATERIALS
www.afm-journal.de

Materials Views
www.MaterialsViews.com

Strain Control of Oxygen Vacancies in Epitaxial Strontium Cobaltite Films

*Jonathan R. Petrie, Chandrima Mitra, Hyoungjeen Jeen, Woo Seok Choi, Tricia L. Meyer, Fernando A. Reboredo, John W. Freeland, Gyula Eres, and Ho Nyung Lee**

The ability to manipulate oxygen anion defects rather than metal cations in complex oxides can facilitate creating new functionalities critical for emerging energy and device technologies. However, the difficulty in activating oxygen at reduced temperatures hinders the deliberate control of important defects, oxygen vacancies. Here, strontium cobaltite ($SrCoO_x$) is used to demonstrate that epitaxial strain is a powerful tool for manipulating the oxygen vacancy concentration even under highly oxidizing environments and at annealing temperatures as low as 300 °C. By applying a small biaxial tensile strain (2%), the oxygen activation energy barrier decreases by ≈30%, resulting in a tunable oxygen deficient steady-state under conditions that would normally fully oxidize unstrained cobaltite. These strain-induced changes in oxygen stoichiometry drive the cobaltite from a ferromagnetic metal towards an antiferromagnetic insulator. The ability to decouple the oxygen vacancy concentration from its typical dependence on the operational environment is useful for effectively designing oxides materials with a specific oxygen stoichiometry.

1. Introduction

Originally seen as undesirable and detrimental to the performance of functional transition metal oxides (TMOs), the formation of oxygen vacancies is becoming increasingly important due to the realization that these same defects can lead to new functional phenomena.[1–3] For instance, incremental changes in oxygen vacancies can leverage large shifts in magnetic, electronic, and catalytic properties in TMOs without introducing possible impurities and segregation associated with heterovalent cation doping.[4–7] Moreover, the functional manipulation of oxygen vacancies is critical for several key information, energy, and environmental technologies, including high T_c superconductors, colossal magnetoresistive materials, oxygen membranes, energy storage, memristors, and other electrochemical devices.[8–12] Traditionally, the concentration and ordering of these vacancies have been dictated by the exposure of oxides to a reducing environment, e.g., oxygen partial pressure and temperature. However, this passive reliance on the environment severely limits the functionality of oxygen vacancies in electrochemical devices, such as batteries and solid oxide fuel cells (SOFCs) that operate at reduced temperatures (<600 °C) far from the optimal conditions for vacancy activation.[13,14] To tailor the content of oxygen vacancies to the increasing number of novel applications that utilize these functional defects, a new method of controlling the oxygen defect concentration is required. An intriguing parameter candidate is strain.

Epitaxial strain in thin film heterostructures is known to critically affect a multitude of physical properties, such as magnetic ordering, electron mobility, ferroelectricity, and superconductivity.[15–19] Recent computational studies have investigated the effects of epitaxial strain on oxygen vacancies in conventional perovskites. While they predict that the activation energies of these vacancies can be tuned by tenths of an eV under modest strains of a few percent, the initial energies of >2 eV render these changes relatively insignificant at reduced temperatures.[20–22] Therefore, to use strain as a new parameter for tuning the oxygen vacancy concentration, oxides with lower activation energies are in high demand.

In this regard, strontium cobaltite, $SrCoO_x$ (SCO), has sparked interest due to the discovery of a low-temperature topotactic transition between the brownmillerite phase $SrCoO_{2.5}$, denoted as BM-SCO, and the perovskite phase $SrCoO_{3-\delta}$, denoted as P-SCO, where $0 \leq \delta \leq 0.25$.[23–25] Due to both the easy intercalation of O^{2-} within BM-SCO offered by ordered vacancy channels (OVCs) and the metastability of Co^{4+} in P-SCO, the cobaltite has exceptionally low oxygen activation energies (<1 eV), amplifying the energetic effects of strain.[26] In addition, deviations in oxygen content from the near-stoichiometric P-SCO result in functional property changes from a ferromagnetic metal to an antiferromagnetic insulator.[23] Furthermore, since the fast, reversible redox reactions offered by these materials promote the Co^{3+}/Co^{4+} redox couple, epitaxial SCO oxygen sponges have revealed enhanced catalytic activities

Dr. J. R. Petrie, Dr. C. Mitra, Dr. H. Jeen,
Dr. W. S. Choi, Dr. T. L. Meyer, Dr. F. A. Reboredo,
Dr. G. Eres, Dr. H. N. Lee
Materials Science and Technology Division
Oak Ridge National Laboratory
Oak Ridge, TN 37831, USA
E-mail: hnlee@ornl.gov
Dr. J. W. Freeland
Advanced Photon Source
Argonne National Laboratory
Argonne, IL 60439, USA

DOI: 10.1002/adfm.201504868

towards CO oxidation at ≈300 °C, making these films attractive for sensors and energy-related devices, such as SOFCs.[23,27] The combination of unique properties and such low energetic thresholds for oxygen control made SCO films an ideal platform for systematically studying strain-induced oxygen nonstoichiometry in these oxides and its ability to influence physical properties.

In this paper, we report that even modest epitaxial strain, specifically tensile strain, can significantly reduce the oxygen activation energy, which effectively leads to a tunable oxygen deficiency even in a highly oxidizing annealing environment. By approaching such an oxygen deficiency from either a topotactically transformed BM-SCO or fully oxidized P-SCO film, the nonstoichiometry is shown as a dynamical equilibrium state. This variation in oxygen stoichiometry under conditions that would normally allow only stoichiometric P-SCO results in tailored and systematic shifts in magnetic and electrical transport properties, demonstrating the control of functionality afforded by strain engineering in perovskite-based oxides.

2. Results and Discussion

2.1. Structural Analysis of Annealed BM-SCO and P-SCO Films

To explore the effects of oxidation on either BM-SCO or fully oxidized, nearly stoichiometric perovskite directly grown in ozone (P-SCO_{ozone}),[23] both sets of films were epitaxially deposited on lattice-mismatched substrates using pulsed laser epitaxy (PLE), as detailed in the Experimental Section. All films had a uniform thickness of 15 nm to ensure no strain relaxation on various perovskite substrates. The substrates included (001) $(LaAlO_3)_{0.3}$–$(SrAl_{0.5}Ta_{0.5}O_3)_{0.7}$ (LSAT), (001) $SrTiO_3$ (STO), (110) $DyScO_3$ (DSO), (110) $GdScO_3$ (GSO), and (001) $KTaO_3$ (KTO). Their pseudocubic parameters range from a_{sub} = 3.868 to 3.989 Å (see **Figure 1**). While BM-SCO is orthorhombic (a_o = 5.574, b_o = 5.447, c_o = 15.745 Å), it will be represented throughout this paper as pseudotetragonal (a_t = 3.905, $c_t/4$ = 3.936 Å).[24] On the other hand, P-SCO (both oxidized BM-SCO and P-SCO_{ozone}) is cubic with a_c = 3.829 Å, leading to substrate-induced lattice mismatches from 1.0 to 4.2%, as shown in Figure 1. Both BM-SCO and P-SCO_{ozone} films were subsequently annealed in-situ at 300 °C in 500 Torr of O_2 for 5 min to explore the effects of strain in a highly oxidizing atmosphere known to convert unstrained SCO to the nearly stoichiometric perovskite.[23,25] As was reported elsewhere,[20,22] such annealing time and environment is known to fully oxidize samples. In either case, oxygen in BM-SCO or P-SCO_{ozone} is respectively intercalated or deintercalated through the OVCs to approach a thermodynamically stable P-SCO state, where stoichiometry under even high oxygen partial pressure is dependent on strain (see Figure 1). XRD reciprocal space mapping confirmed that brownmillerite and perovskite films used here were coherently strained (see Figures S1 and S2, Supporting Information).

Figure 1a shows an example of our observation that strain can modulate oxygen stoichiometry in epitaxial P-SCO films that have undergone topotactic oxidation. The XRD θ–2θ scans around the P-SCO 002 peak for annealed BM-SCO on various substrates are given. The θ–2θ scans for annealed P-SCO_{ozone} are virtually identical. Each perovskite peak is clearly defined with Kiessig fringes that verify the superior film quality. However, upon careful inspection of the out-of-plane lattice constant, the monotonic shift in the out-of-plane lattice parameter with tensile strain cannot be simply understood through a Poisson-type contraction due to substrate-induced tensile strain. Therefore, we further considered the possibility of lattice expansion due to increased vacancy formation as the film deviates from the stoichiometric δ = 0 P-SCO phase in $SrCoO_{3-\delta}$.[22,28] We compared the unit cell volume of these annealed films to that of the as-grown P-SCO_{ozone} films (see Figure S3 in the Supporting Information for θ–2θ scans), which have essentially stoichiometric concentrations of oxygen.[23,29,30] As seen

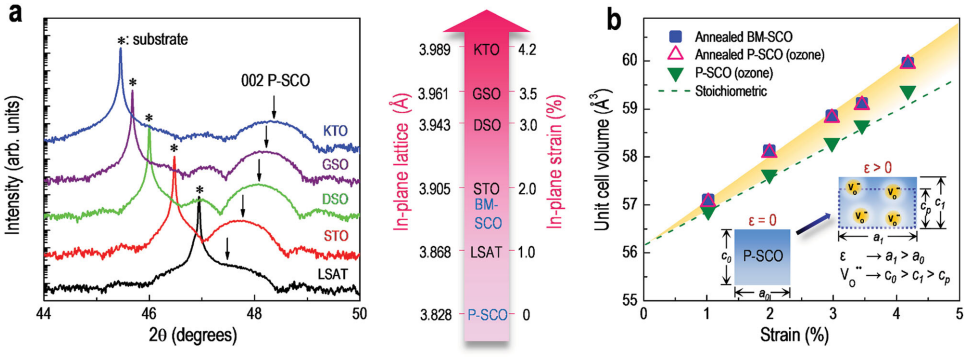

Figure 1. Strain control of oxygen stoichiometry in epitaxial P-SCO. a) XRD θ–2θ scans around the 002 peak of topotactically oxidized P-SCO films on different substrates. Substrate peaks are noted by asterisks (*). In-plane lattice parameters and biaxial strain applied to P-SCO are provided adjacent to the scan. b) As the in-plane parameter a_0 is stretched to a_1 due to tensile strain, there is the expected shift in the 002 peak from c_0 to the contracted c_1 out-of-plane parameter. However, c_1 is larger than would be expected from a Poisson contraction (c_p and dotted box) of stoichiometric P-SCO. To deconvolute the effects of strain and vacancy formation, unit cell volumes as a function of biaxial strain for either annealed BM-SCO or P-SCO_{ozone} films are given. The similarity among the annealed films indicates an equilibrium oxygen stoichiometry attained through either the deintercalation or intercalation of oxygen. The lattice volume sizes are compared to the ones of fully oxidized $SrCoO_x$ ($x \geq 2.9$) (P-SCO_{ozone}) films from ozone growth, which revealed a Poisson ratio ν = 0.26 (dashed line). As denoted by the shaded region, the higher the tensile strain, the higher the volume deviation from the dashed line, indicating an increase in oxygen vacancies.

in Figure 1b, the unit cell volume of the P-SCO$_{ozone}$ films increased monotonically with strain for all but the $\varepsilon = 4.2\%$ film, which may be due to a slight change in oxygen stoichiometry or phase transition.[31] This increase was readily fit to a line ascribing all linear expansion to a Poisson ratio of $\nu \approx 0.26$, which is a common value associated with cobaltites.[32] Similarly, the BM-SCO had a $\nu \approx 0.30$, as seen in Figure S4 (Supporting Information). However, the topotactically oxidized P-SCO films exhibited a larger lattice volume than that of as-grown P-SCO$_{ozone}$. This deviation becomes more pronounced when the tensile strain increases. As summarized in Figure 1b, this increased unit cell volume is observed from P-SCO samples prepared by either annealing BM-SCO or P-SCO$_{ozone}$, indicating a steady-state vacancy concentration attained through, respectively, either the intercalation or deintercalation of oxygen. As the increase in the oxygen vacancies often results in lattice expansion for perovskite-typed complex oxides, we primarily attribute this deviation to the greater oxygen deficiency in the films with tensile strain;[28] otherwise, an unrealistic $\nu = 0.17$ would be required from fully oxygenated films to fit the experimental data.[33]

2.2. Oxygen Stoichiometry Changes probed by X-Ray Absorption Spectroscopy

To confirm that the oxygen stoichiometry in the film varies as the tensile strain is increased, we investigated the topotactically oxidized P-SCO films by X-ray absorption spectroscopy (XAS) using both the O *K*- and Co *L*-edges. As seen in **Figure 2**a, there are two peaks of note in the prepeak region of the O *K*-edge. These peaks are labeled A and B and are linked to Co 3*d*–O 2*p* hybridization from hole states associated, respectively, with either fully oxidized or partially oxidized coordination.[34] While the intensity of Peak B increases under tensile strain with oxygen loss, peak A substantially diminishes as less intercalated oxygen translates into an oxygen deficient state. Peak A also shifts to higher photon energies with oxygen loss as a result of negative charge-transfer.[35] The shift of 0.2 eV as strain increases to 4.2% is consistent with the transition from $SrCoO_{2.9}$ to $SrCoO_{2.75}$ determined in previous studies for bulk P-SCO.[36]

An investigation of the Co-*L* edge in Figure 2b also indicates a changing valence state with increasing amounts of oxygen vacancies at higher tensile strains. The shift in intensity of the Co-$L_{2,3}$ peaks towards lower energies confirms that there is indeed a decrease in the average transition metal valency from Co^{4+} with increasing strain. The chemical shift in the Co L_2 edge between the $\varepsilon = 1.0$ and 4.2% films is –0.3 eV. A related –1 eV shift in the Co L_2 edge can be seen in the $(La_{1-x}Sr_x)CoO_3$ system when one electron is transferred away from Co as the Sr concentration varies from $x = 1$ to $x = 0$.[37] Using this shift, we can estimate a transfer here of up to 0.3 e^-, which is compatible with $\Delta\delta \leq 0.15$ as the equilibrium state transitions from $SrCoO_{2.9}$ to $SrCoO_{2.75}$ with tensile strain. Quantification of the oxygen non-stoichiometry is given in **Figure 3**. The estimates of oxygen deficiency were obtained from comparing structural data (unit cell volume)[29,30] and spectroscopic peak shifts (O-*K* and Co-*L* edges)[34,37] to previous studies.

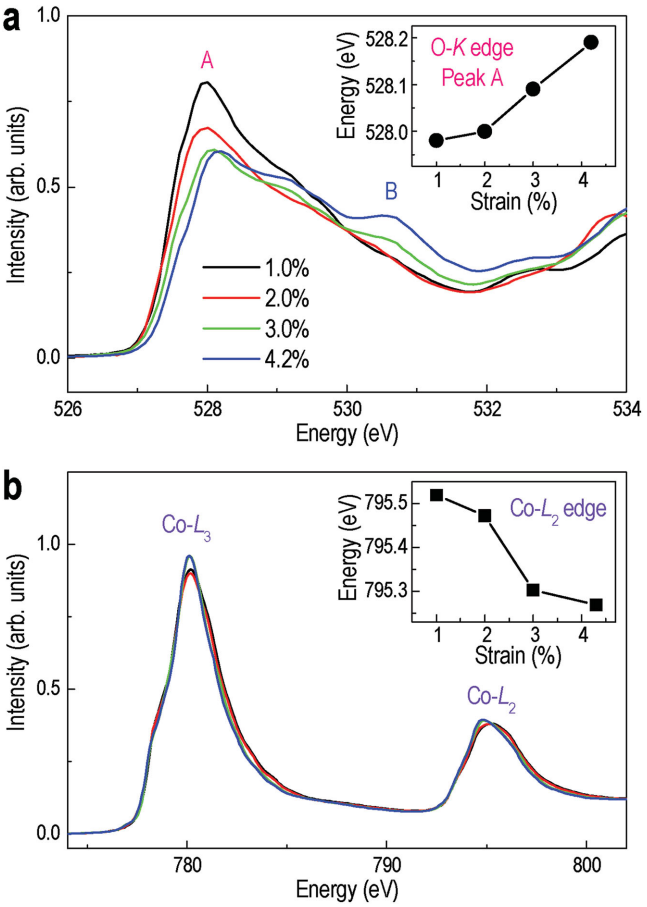

Figure 2. Evidence for preferential oxygen loss in tensile strained P-SCO. a) XAS O-*K* edge of annealed P-SCO films on LSAT ($\varepsilon = 1.0\%$) through KTO ($\varepsilon = 4.2\%$) substrates. Peaks at ≈528 eV (A) and ≈530.5 eV (B) correspond to Co3*d*-O2*p* hybridization, respectively, associated with either fully oxidized or partially oxidized Co coordination. The inset shows the chemical shift of Peak A with increasing tensile strain, which corresponds to a shift from $SrCoO_{2.9}$ to $SrCoO_{2.75}$. b) The Co-$L_{2,3}$ edges indicate the shift in Co valency from Co^{4+} to Co^{3+} as vacancies are induced by tensile strain. Quantitatively shown in the inset, the shift of the Co-L_2 edge corroborates the same change in stoichiometry as the O-*K* edge.

2.3. Evolution of Magnetic and Electrical Transport Properties with Strain

Varying the oxygen vacancy content through strain has powerful effects on the magnetic and electronic properties of the cobaltite. It is already theoretically predicted that strain can diminish the ferromagnetic and metallic states of stoichiometric P-SCO due to reduction in the orbital overlap.[38,39] However, as seen in the magnetic and electrical transport properties in **Figure 4**, increasing oxygen non-stoichiometry complements strain in driving the transition from a ferromagnetic metal to an antiferromagnetic insulator. To decouple the effects of pure strain from the effects of strain-induced changes in the oxygen stoichiometry, magnetization and transport properties are shown for both the as-grown, fully-oxidized P-SCO$_{ozone}$ as well as the non-stoichiometric annealed P-SCO. Figure 4 a,d shows the respective magnetic moments of the P-SCO$_{ozone}$ and annealed P-SCO films as a function of

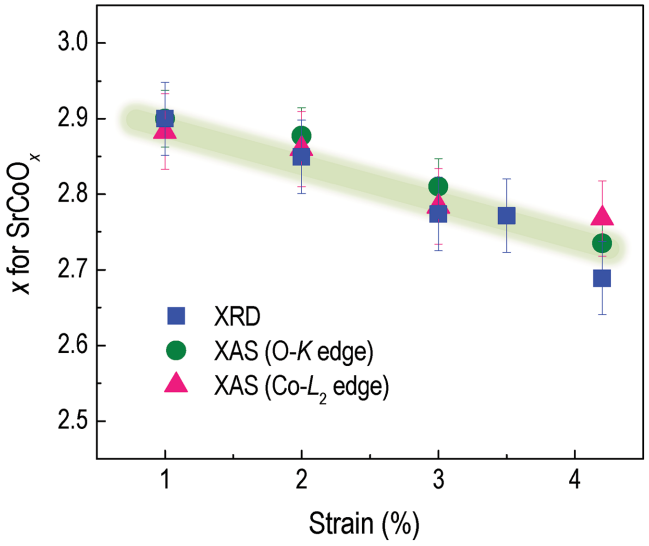

Figure 3. Oxygen deficiency in tensile strained P-SCO. Oxygen non-stoichiometry x in $SrCoO_x$ determined by comparing XRD-based volume changes and peak position shifts of XAS O-K and Co-L_2 edges to the literature values.[29,30,34,37] From this combined data set, x is found to range from just below 3 to 2.75 as tensile strain increases from $\varepsilon = 1\%$ to $\varepsilon = 4.2\%$

magnetic field at 10 K. Due to the large magnetic moments of the paramagnetic DSO and GSO substrates, magnetization data of thin films on those substrates are not shown. As expected from theoretical studies, the saturation magnetization M_s of the fully-oxidized P-SCO_{ozone} slightly decreases after $\varepsilon = 2\%$ due to lessening of the orbital overlap.[38,39] However, the annealed P-SCO shows a much more dramatic decrease in M_s, declining from 2.3 μ_B/Co for the $\varepsilon = 1\%$ case to 0.1 μ_B/Co for $\varepsilon = 4.2\%$. The M_s as a function of temperature in Figure 4 b,e also shows the weakening of the ferromagnetic properties from a Curie temperature, T_c, above 230 K for all strained P-SCO_{ozone} to a range from ≈220 to 160 K on annealed SCO, decreasing with strain. Furthermore, according to a recent bulk study[40] $T_c \approx 160$, 220, and 280 respectively indicated off-stoichiometric P-SCO phases $SrCoO_{2.75}$, $SrCoO_{2.90}$, and $SrCoO_3$. Therefore, the reduction of T_c in our annealed P-SCO thin films samples suggests a change from $\delta \approx 0.1$ for $\varepsilon = 1\%$ to $\delta \approx 0.25$ for $\varepsilon = 4.2\%$.

Moreover, electrical *dc* transport measurements in Figure 4 c,f show a correlation with the changing oxygen stoichiometry due to strain. As seen from the electrical transport data in Figure 4c, P-SCO_{ozone} films with strains of at most $\varepsilon = 2.0\%$ are metallic and indicate increasing insulating behavior with tensile strain due to increased localization of carriers.[38,39] When comparing these films to the annealed P-SCO in Figure 4f, the annealed P-SCO films reveal significantly increased resistivities due to strain-induced changes in oxygen stoichiometry. In fact, the only substrate on which the annealed P-SCO film is metallic is LSAT, which induces a strain of only ≈1% in the film. Since it has been shown that the double exchange mechanism thought responsible for the metallic behavior of P-SCO is disrupted when $\delta = 0.1$, we can place an upper bound on δ at this level when 1% tensile strain is supplied to the film.[36,41] At mismatches that induce even greater tensile strains, the transition to an increasingly insulating nature implies that $\delta > 0.1$ and that δ is increasing with such strain. Consistent with the XAS and magnetization data, none of the films (even with strain) exhibit behaviors that imply $\delta > 0.25$ or the BM-SCO phase; in comparison to the resistivity of a previously deposited 14 nm BM-SCO film on STO, all annealed P-SCO films have values orders of magnitude lower up to room temperature. In addition, the derived activation energy from the transport measurements for conductive species increases to only 87 meV for P-SCO under 4.2% strain compared to 240 meV for the BM-SCO film over a similar temperature range. This again suggests that while the films are increasingly oxygen deficient, no tensile strain was sufficient to topotactically transform the P-SCO film back to BM-SCO under these conditions.

This electronic trend has also been observed in our prior study;[24] however, the origin for the less conducting behavior under tensile strain has not been completely understood. Indeed, while the systematic trend is obvious, the more insulating nature from the P-SCO films compared to P-SCO_{ozone} indicates that their carrier transport is strongly influenced by the change in strain-induced carrier concentration owing to the loss of oxygen. However, an optical spectroscopy study (see Figure S5 in the Supporting Information) revealed that even the highly insulating P-SCO film on STO maintains similar spectral features as the metallic P-SCO on LSAT, which has clear Drude features.[25] Thus, we conclude that the P-SCO thin films are at the verge of the percolation limit with a possible coexistence of metallic (P-SCO) and insulating (BM-SCO) phases. A similar trend was reported in manganite bulk and thin film samples, which also showed a discrepancy between optical and dc transport data.[42]

2.4. Strain Control of Oxygen Activation Energy and Formation Enthalpy

To understand the experimental observation of the strong coupling between strain and oxygen stoichiometry, we performed first-principles density functional theory (DFT) calculations.[26,43–46] We specifically computed two quantities as a function of strain (see Supporting Information for details).[47] The first is the intercalation formation enthalpy, H_i, to intercalate an oxygen atom into one of the vacancy sites, which is the point of lowest energy in the system. The other is the activation energy barrier, E_a, which is the energy required for an oxygen atom to diffuse from one vacancy site to another along OVCs in the open network structure.[48] As seen in **Figure 5**a, in diffusing from one vacancy site to the other along the [010] direction in the channel, O^{2-} crosses an intermediate saddle point, H_{saddle}, which is the point of highest energy in the system.[13] This results in E_a being composed of the difference between H_{saddle} and H_i. While H_{saddle} only slightly lowers with tensile strain, H_i significantly increases with tensile strain due to changes in the stabilizing effects of hybridization between Co 3*d* and O 2*p*, which are dependent on the Co-O bond length.[20]

As shown in Figure 5b, the net effect of such tensile strain reduces E_a, whereas it is raised by compressive strain.

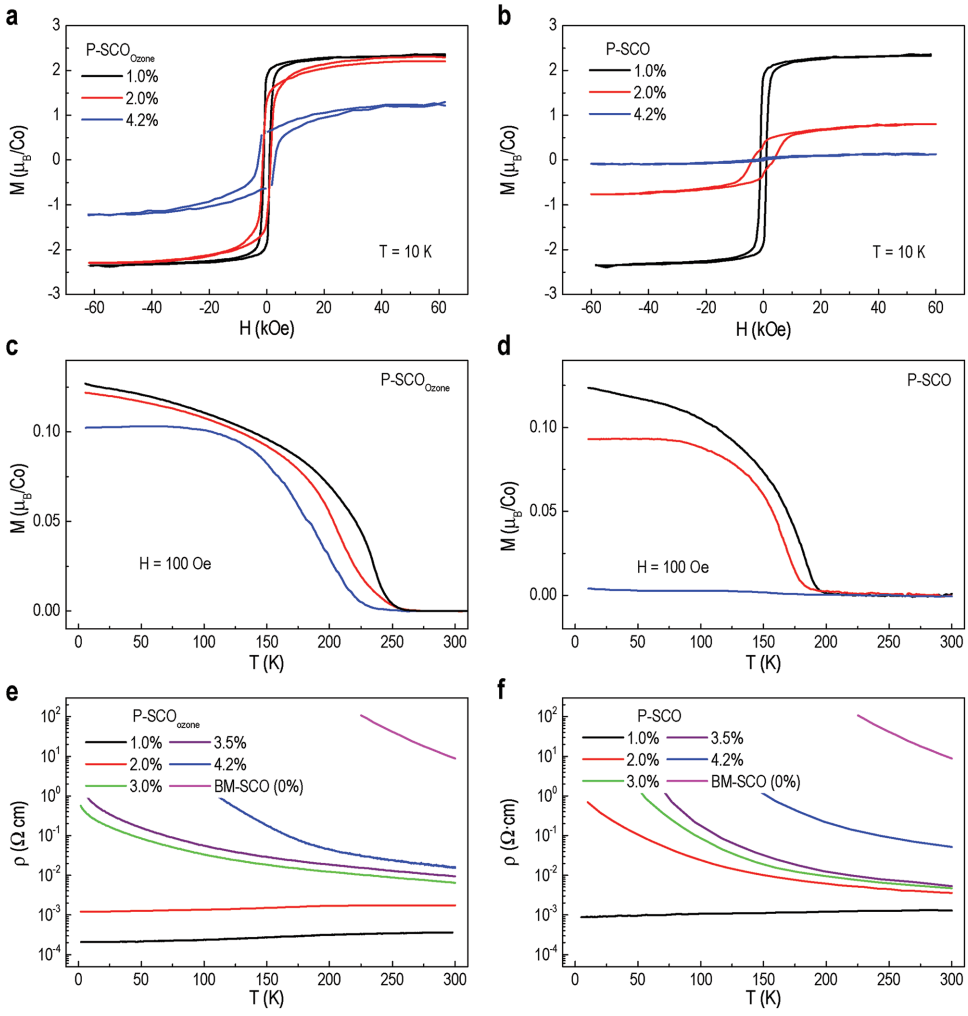

Figure 4. Strain dependent physical properties. a–c) The magnetization and electrical transport of P-SCO$_{ozone}$ are shown in the top panels, d–f) while those of annealed P-SCO are displayed in the bottom panels. We note that the growth in highly oxidizing ambient using ozone could improve the oxygen stoichiometry. Tensile strain results in deterioration of the ferromagnetic metallic ground state, and the addition of strain-induced changes in oxygen stoichiometry radically drives the P-SCO toward becoming an antiferromagnetic insulator. As-grown BM-SCO on STO is included as a reference, putting an upper boundary on the oxygen deficiency for P-SCO.

It is worth stressing that by applying only a 2% tensile strain, one can reduce the activation energy barrier by ≈30%. Such declines immediately suggest benefits towards ionic conduction for SOFCs and oxygen sensor applications.[2–4] Concurrent with the strain-induced changes in E_a, as shown in Figure 3b, H_i rises with tensile strain and falls with compressive strain, respectively suggesting either greater or smaller thermodynamic oxygen instability. Both values indicate that the application of tensile strain significantly facilitates oxygen vacancy generation, whereas compressive strain prevents the system from losing oxygen, due to shifts in the enthalpy of the vacancy sites. By controlling the energetics of the vacancy sites through strain, shifts due to environmental influences can be minimized and oxygen vacancy dependent properties, such as conductivity and magnetism, adjusted in conditions that would fully oxidize the perovskite towards a simple ferromagnetic metal.

3. Conclusion

In summary, this work shows that by growing epitaxially strained $SrCoO_{3-\delta}$ thin films, we can tailor oxygen non-stoichiometry crucial for functionality simply by applying tensile strain to lower the equilibrium oxygen concentration. We attribute the phenomenon of easier oxygen loss in tensile-strained films to reduced oxygen activation energy from weakened Co-O bonding. Remarkably, this approach is capable of controlling oxygen vacancies even in highly oxidizing environments, producing large changes in magnetic and electronic properties suitable for sensors and devices designed to work in oxidizing conditions and reduced temperatures. With the discovery that tensile strain dictates the oxygen stoichiometry by controlling the activation energies in these perovskite-based strontium cobaltites, deterministic control over physical and electrochemical properties can be envisioned. Thus, this

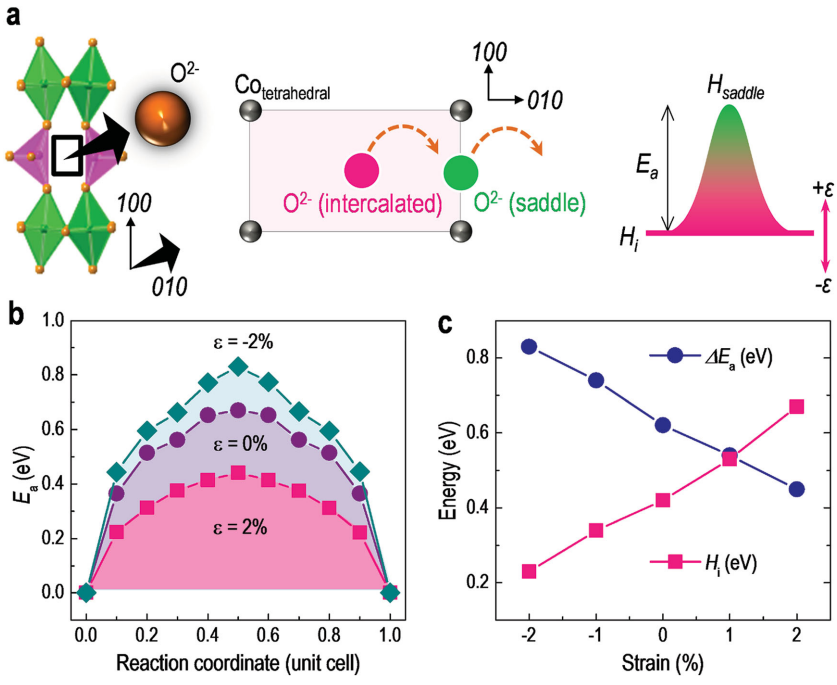

Figure 5. Strain dependent oxygen activation. a) A schematic indicating the path and energy barriers for oxygen ion movement in BM-SCO through the oxygen vacancy channels (OVCs) when undergoing a topotactic oxidation to P-SCO. While the intercalation enthalpy, H_i, at the vacancy sites changes significantly with strain, the point of highest energy, the saddle point (H_{saddle}), is not considerably affected. The difference between the two is the activation energy (E_a). b) As an oxygen ion is moved from one intercalation site to another along the [010] direction of the OVC, the E_a increases as the strain state trends from +2% to –2%. c) A summary of the activation energy barrier (ΔE_a) and intercalation enthalpy (H_i) as a function of strain, showing that tensile strain facilitates oxygen movement through the OVCs and reduces the stability of oxygen intercalation (leading to vacancy formation), whereas compressive strain preferentially immobilizes oxygen. The OVC (□) is within the tetrahedral (pink) layer, which is bounded by the octahedral layers (green).

observation of strain-engineered oxygen defects opens up a new route for designing novel functional oxides using strain as the key tuning parameter.

4. Experimental Section

Thin Film Synthesis: Epitaxial films of BM-SCO and P-SCO were grown 15 nm thick on various substrates through pulsed laser epitaxy (PLE). Similar to previous work,[23–25] the BM-SCO growth temperature, oxygen partial pressure, laser fluence, and repetition rate were fixed at 750 °C, 100 mTorr, 1.5 J cm^{-2}, and 5 Hz, respectively. The BM-SCO films were cooled *in situ* under 100 mTorr of O_2 to 300 °C before introducing 500 Torr O_2 for 5 minutes into the chamber to topotactically oxidize the films to P-SCO. P-SCO$_{ozone}$ films were grown under the same conditions with the exception of the partial pressure, which was a 200 mTorr of a mix of O_2+O_3 (5%). The P-SCO$_{ozone}$ films were cooled *in-situ* under the same 200 mtorr partial pressure to 300 °C before introducing 500 Torr O_2 for 5 minutes into the chamber oxidize the films. All films were characterized immediately after deposition or annealing.

Characterization of Structural and Physical Properties: The sample structure was characterized with a high-resolution four-circle XRD. Temperature-dependent *dc* transport measurements were conducted using the van der Pauw geometry with a 14 T Physical Property Measurement System (PPMS). Optical spectroscopy was performed using a spectroscopic ellipsometer between 1.25 and 5.00 eV at an incident angle of 70°. A simple two-layer model (film/substrate) was used to extract dielectric functions and optical conductivity. Valence state and oxygen stoichiometry via XAS were performed at the beamline 4-ID-C of the Advanced Photon Source at Argonne National Laboratory.

DFT Calculations: All modeling calculations have been performed within density functional theory (DFT) employing the Vienna Ab-initio Simulations Package (VASP) code. We have used 2 × 2 × 1 supercells for all calculations containing 144 atoms. Projector-augmented wave pseudopotentials have been used with an energy cut of 600 eV. The activation energy (E_a) barriers (ΔE_a) for oxygen ions and the intermediate transition states have been computed using the Nudged Elastic Band method as implemented in the VASP code. The energy barriers have been optimized until the forces on each image were converged to 0.004 eV Å^{-1}. In order to account for strong correlations, the cobalt *d* orbitals are treated within the local spin density (LSD) approximation with Hubbard *U* corrections. A *U* value of 7.5 eV was chosen, the electronic structure of which matched closely to those computed with the Hybrid Scuzeria Ernzerhof functional. Further details can be found in the Supporting Information and in previous work.[26]

Supporting Information

Supporting Information is available from the Wiley Online Library or from the author.

Acknowledgements

This work was supported by the U.S. Department of Energy, Office of Science, Basic Energy Sciences, Materials Science and Engineering Division. Use of the Advanced Photon Source was supported by the U.S. Department of Energy, Office of Science, under Contract No. DE-AC02-06CH11357.

Received: November 13, 2015
Published online: January 25, 2016

[1] J. Mannhart, D. G. Schlom, *Nature* **2004**, *430*, 620.
[2] S. V. Kalinin, A. Borisevich, D. Fong, *ACS Nano* **2012**, *6*, 10423.
[3] J. Maier, *Nat. Mater.* **2005**, *4*, 805.
[4] B. Yildiz, *MRS Bull.* **2014**, *39*, 147.
[5] U. Bauer, L. Yao, A. J. Tan, P. Agrawal, S. Emori, H. L. Tuller, S. van Dijken, G. S. D. Beach, *Nat. Mater.* **2014**, *14*, 174.
[6] S. J. Skinner, J. A. Kilner, *Mater. Today* **2003**, *6*, 30.
[7] N. H. Hong, J. Sakai, N. Poirot, V. Brize, *Phys. Rev. B* **2006**, *73*, 132404.
[8] D. B. Strukov, G. S. Snider, D. R. Stewart, R. S. Williams, *Nature* **2008**, *453*, 80.
[9] J. Jeong, N. Aetukuri, T. Graf, T. D. Schladt, M. G. Samant, S. S. P. Parkin, *Science* **2013**, *339*, 1402.
[10] J. G. Bednorz, K. A. Müller, *Z. Phys. B: Condens. Matter* **1986**, *64*, 189.
[11] A. P. Ramirez, *J. Phys.: Condens. Matter* **1997**, *9*, 8171.
[12] R. Waser, R. Dittmann, G. Staikov, K. Szot, *Adv. Mater.* **2009**, *21*, 2632.

[13] P. Pasierb, S. Komornicki, M. Rekas, *J. Phys. Chem. Solids* **1999**, *60*, 1835.
[14] M. Kubicek, Z. Cai, W. Ma, B. Yildiz, H. Hutter, J. Fleig, *ACS Nano* **2013**, *7*, 3276.
[15] H. M. Manasevit, I. S. Gergis, A. B. Jones, *Appl. Phys. Lett.* **1982**, *41*, 464.
[16] C. Ederer, N. A. Spaldin, *Phys. Rev. B* **2005**, *71*, 224103.
[17] J. P. Locquet, J. Perret, J. Fompeyrine, E. Machler, J. W. Seo, G. Van Tendeloo, *Nature* **1998**, *394*, 453.
[18] M. Mavrikakis, B. Hammer, J. K. Norskov, *Phys. Rev. Lett.* **1998**, *81*, 2819.
[19] W. S. Choi, J.-H. Kwon, H. Jeen, J. E. Hamann-Borrero, A. Radi, S. Macke, R. Sutarto, F. He, G. A. Sawatzky, V. Hinkov, M. Kim, H. N. Lee, *Nano Lett.* **2012**, *12*, 4966.
[20] A. Kushima, S. Yip, B. Yildiz, *Phys. Rev. B* **2010**, *82*, 115435.
[21] L.-Y. Gan, S. O. Akande, U. Schwingenschlogl, *J. Mater. Chem. A* **2014**, *2*, 19733.
[22] U. Aschauer, R. Pfenninger, S. M. Selbach, T. Grande, N. A. Spaldin, *Phys. Rev. B* **2013**, *88*, 054111.
[23] H. Jeen, W. S. Choi, M. D. Biegalski, C. M. Folkman, I. C. Tung, D. D. Fong, J. W. Freeland, D. Shin, H. Ohta, M. F. Chisholm, H. N. Lee, *Nat. Mater.* **2013**, *12*, 1057.
[24] H. Jeen, W. S. Choi, J. W. Freeland, H. Ohta, C. U. Jung, H. N. Lee, *Adv. Mater.* **2013**, *25*, 3651.
[25] W. S. Choi, H. Jeen, J. H. Lee, S. S. A. Seo, V. R. Cooper, K. M. Rabe, H. N. Lee, *Phys. Rev. Lett.* **2013**, *111*, 097401.
[26] C. Mitra, T. Meyer, H. N. Lee, F. A. Reboredo, *J. Chem. Phys.* **2014**, *141*, 084710.
[27] H. Jeen, Z. Bi, W. S. Choi, M. F. Chisholm, C. A. Bridges, M. P. Paranthaman, H. N. Lee, *Adv. Mater.* **2013**, *25*, 6459.
[28] C. Yu, S. B. Adler, *Chem. Mater.* **2005**, *17*, 4537.
[29] R. Le Toquin, W. Paulus, A. Cousson, C. Prestipino, C. Lamberti, *J. Am. Chem. Soc.* **2006**, *128*, 13161.
[30] A. Nemudry, P. Rudolf, R. Schoellhorn, *Chem. Mater.* **1996**, *8*, 2232.
[31] S. Hu, Z. Yue, J. S. Lim, S. J. Callori, J. Bertinshaw, A. Ikeda-Ohno, T. Ohkochi, C. H. Yang, X. Wang, C. Ulrich, J. Seidel, *Adv. Mater. Interfaces* **2015**, *2*, 140405.
[32] D. Fuchs, T. Schwarz, O. Morán, P. Schweiss, R. Schneider, *Phys. Rev. B* **2005**, *71*, 092406.
[33] C. W. Huang, W. Ren, V. C. Nguyen, Z. Chen, J. Wang, T. Sritharan, L. Chen, *Adv. Mater.* **2012**, *24*, 4170.
[34] L. Karvonen, M. Valkeapaa, R.-S. Liu, J.-M. Chen, H. Yamauchi, M. Karppinen, *Chem. Mater.* **2010**, *22*, 70.
[35] J. Kuneš, V. Krápek, N. Parragh, G. Sangiovanni, A. Toschi, A. V. Kozhevnikov, *Phys. Rev. Lett.* **2012**, *109*, 117206.
[36] S. Balamurugan, K. Yamaura, A. B. Karki, D. P. Young, M. Arai, E. Takayama-Muromachi, *Phys. Rev. B* **2006**, *74*, 172406.
[37] Z. Hu, C. Grazioli, M. Knupfer, M. S. Golden, J. Fink, P. Mahadevan, A. Kumar, S. Ray, D. D. Sarma, S. A. Warda, D. Reinen, S. Kawasaki, M. Takano, C. Schüssler-Langeheine, C. Mazumdar, G. Kaindl, *J. Alloys Compd.* **2002**, *343*, 5.
[38] J. H. Lee, K. M. Rabe, *Phys. Rev. Lett.* **2011**, *107*, 067601.
[39] C. Mitra, R. S. Fishman, S. Okamoto, H. N. Lee, F. A. Reboredo, *J. Phys.: Condens. Matter* **2014**, *26*, 036004.
[40] C. K. Xie, Y. F. Nie, B. O. Wells, J. I. Budnick, W. A. Hines, B. Dabrowski, *Appl. Phys. Lett.* **2011**, *99*, 052503.
[41] M. Bajdich, M. García-Mota, A. Vojvodic, J. K. Nørskov, A. T. Bell, *J. Am. Chem. Soc.* **2013**, *135*, 13521.
[42] K. H. Kim, J. Y. Gu, H. S. Choi, D. J. Eom, J. H. Jung, T. W. Noh, *Phys. Rev. B* **1997**, *55*, 4023.
[43] P. E. Blochl, *Phys. Rev. B* **1994**, *50*, 17953.
[44] G. Henkelman, H. Jansson, *J. Chem. Phys.* **2000**, *113*, 9978.
[45] G. Henkelman, B. P. Uberuaga, H. Jansson, *J. Chem. Phys.* **2000**, *113*, 9901.
[46] S. L. Dudarev, G. A. Botton, S. Y. Savrasov, C. J. Humphreys, A. P. Sutton, *Phys. Rev. B* **1998**, *57*, 1505.
[47] S. B. Zhang, J. E. Northrup, *Phys. Rev. Lett.* **1991**, *67*, 2339.
[48] C. Mitra, R. S. Fishman, S. Okamoto, H. N. Lee, F. A. Reboredo, *J. Phys.: Condens. Matter* **2014**, *26*, 036004.